Desalination and Water Treatment
www.deswater.com

doi: 10.5004/dwt.2019.24000

155 (2019) 55–63
July

Corncob waste activated with different pore formers for capacitive deionization (CDI) materials

Lang Lang, Xiao-min Hu*, Yan Zhao*, Jun Wang, Hong Lin

School of Resources and Civil Engineering, Northeastern University, Shenyang 110819, China, Tel./Fax: 86-24-83689128; email: hxmin_jj@163.com (X.-min Hu), Tel. 86-13897901029; email: 21052516@qq.com (Y. Zhao), Tel. 86-18842488202; email: 976832174@qq.com (L. Lang), Tel. 86-18640524717; email: 372609289@qq.com (J. Wang), Tel. 86-13897901029; email: 568233331@qq.com (H. Lin)

Received 13 August 2018; Accepted 20 February 2019

ABSTRACT

As a new desalination technology, capacitive deionization (CDI) has made continuous progress in recent years. This paper explores possible resource utilization channels for corncob waste to prepare capacitive deionized plate materials. Using corncob waste as a matrix, porous materials were prepared by high-temperature insulation from oxygen. The specific surface area of the resulting carbon material was 1,267.9 $m^2 g^{-1}$, and a capacitance of 145.5 F g^{-1} was achieved in a three-electrode system; the desorption capacity was 16.9 mg g, close to the performance of high-performance materials such as graphene. CDI uses low-cost and waste recycling materials. In the present study, different effects of K_2FeO_4 and KOH as pore formers on the micro-morphology and chemical structure of the material were compared. The corncob-based carbon materials obtained from K_2FeO_4 and KOH met the basic requirements of the capacitive deionized plate material, whereas K_2FeO_4 increased the degree of graphitization of corncob carbon materials; the corncob-based bio char produced from the K_2FeO_4 pores helped to shorten the time of one adsorption cycle, but the cost is slightly higher than that of the KOH hole. Under different requirements, K_2FeO_4 and KOH are promising as pore-forming agents for corncob CDI electrodes. The cycling performance verified that the carbon materials prepared in the previous process performed well during the desorption process and recycling process, which can meet the needs of repeated use, and corncob waste is a promising resource for capacitive deionization plate materials.

Keywords: Capacitor deionization; Activated corncob carbon; Pore-forming agent; Graphitization

1. Introduction

Removing ionic compounds dissolved in water is an important step in the process of water treatment. With the flourishing development of carbon materials and supercapacitors in recent years, a new tool called capacitive deionization (CDI) is emerging as a competitive technology that consumes less energy and is easy to maintain compared with reverse osmosis, multi-stage flash distillation and multi-effect distillation [1–4]. Capacitance deionization devices are based on the principles of supercapacitors, which use carbon materials with a highly specific surface area to coat the electrode plate. Capacitor deionization device migrates ions to the electrode plate by applying voltage [1].Double-layer capacitance is formed at the plate, which can store large amounts of ions that are removed from solution. The nature of the carbon materials used in the plates determines the capacity of the plates, and the capacitance of the plate is key to ion removal [5–15].

Recently, CDI has made substantial progress in improving technologies, such as MCDI and FCDI [16,17]. Moreover, energy recycling studies have been developed [18–20].

* Corresponding authors.

However, there are still many difficulties due to low-cost applications. Electrode material applications still have room for improvement. Some well-made electrode materials, such as graphene and carbon aerogel, have high raw material costs, and the process of their production requires complex chemical reactions, and some of the by-products involved in production pollute the environment. However, using a CDI device to remove ions from water involves the preparation of a large amount of high-performance activated carbon. The cost of carbon material production needs to be considered as one of the factors in the preparation of the CDI device.

Based on cost and utility considerations, bio-based carbon nano materials may be the most suitable materials for CDI electrodes. Many studies have noted that bio-based carbon materials can also achieve superior performance and have verified that the bio-based carbon materials used as CDI electrodes for desalination performed well [5,21–23,24,25].

The treatment of some biological wastes, such as plant stalks and corncobs, is a problem in environmental governance. Burning these wastes in place causes severe pollution in the atmosphere. Studies demonstrate that some biological wastes can be used as supercapacitor carbon materials directly after some treatment [26]. Moreover, the CDI device with a principle similar to the supercapacitor requires more green carbon materials. Our study aims to find a simpler preparation method for biochar materials suitable for a CDI device.

The choice of pore-forming agents is crucial for leaving more pores of suitable size. In the CDI process, the performance requirements of the carbon material are higher. The process requires that the carbon coating of electrodes has a higher degree of graphitization, a highly specific surface area and a complex mesoporous structure. Due to the original complex composition and structure of biomass, different chemical activation methods have different effects on the structure of the resulting carbon material [27]. The essence of chemical activation is to form micropores through a series of cross linking condensation reactions by embedding chemical reagents into the internal structure of carbon particles. The commonly used activators are KOH, $ZnCl_2$, Na_2CO_3, H_3PO_4 [28–32]. The specific processes and sequences of activation reactions are still controversial according to different papers. However, many studies have shown that the KOH activation method can be used to make active carbon, with a highly specific surface area and homogeneous pore, that plays an important role in the field of supercapacitors [21,28].The $ZnCl_2$ activation method in the actual production of more supercapacitors does not produce alkali steam, as the equipment requirements are not as high as those of the KOH activation method [30].Recently, Young Gong [33] using bamboo as raw material and potassium ferrate as a one-step porous agent, achieved uniform rich micropores and a high degree of graphitization, with a capacitance of 222.0 F g^{-1}.

In this work, we contrasted three handy chemical activation processes by KOH, $ZnCl_2$ and K_2FeO_4 for the preparation of highly specific surface area activated carbon that use corncob waste as the precursor. The three kinds of pore-forming agents we used showed different characteristics in the process of making corncob waste into CDI electrode materials.

In this paper, a chemical living method for preparing highly specific surface area activated carbon for corncob waste is discussed and was used for the electrode material of the capacitor deionization process; the waste resource was utilized, and the CDI electrode material was prepared at low cost. The effects of different pore-making agents on the preparation of corncob biochar are described below; the maximum surface area of biochar reached 1,267.9 m^2 g^{-1}, the capacitance was 145.5 F g^{-1} in the three-electrode system, and the adsorption capacity reached 16.9 mg L^{-1} in 500 mg L^{-1} brine. The plate material obtained by the hole-making agent achieved desalting balance faster. The scheme of this experiment effectively yielded a low-cost, high-performance capacitance ion plate material, with the advantages of the preparation process using both KOH and K_2FeO_4 as a hole-making agent.

2. Experimental setup

2.1. Preparation of activated corncob carbon (ACC)

The original corncob wastes were taken from farmland in the suburbs of Shenyang, Liaoning, China. We picked the corncobs after the corn was harvested and stripped of corn kernels. We put the corncobs into a small electric grinder for five minutes and then used a 40-mesh sieve to sieve corncob powder. The corncob powder obtained was repeatedly washed with alcohol and deionized water and dried overnight at 80°C. Next, 10 g of the dried powder was pyrolyzed in a tubular furnace(HF-kejingOTF-1200X) at 400°C for 2 h, with a heating rate of 5ºC min^{-1} in a nitrogen atmosphere. The resultant carbon powder was obtained and denoted corncob carbon (CC).

The obtained carbon powder was added to KOH, $ZnCl_2$, K_2FeO_4 at a mass ratio of 1:1, 1:2.4 and 1:1.8, respectively; the mass ratio ensures that the molar ratio of the main components of each activator is the same and that an appropriate amount of deionized water was added and stirred for 5 h, followed by drying overnight in a 100° drying oven. The dried samples were labelled CC-1, CC-2, CC-3, and the unprocessed corncob carbon was marked CC-0. These samples were put into a tubular furnace and activated at 800°C for 2 h, with a heating rate of 5°C min^{-1} in a nitrogen atmosphere. The resulting samples were washed multiple times with diluted hydrochloric acid and deionized water to remove hole-making agent impurities, followed by drying at 100°C overnight. The samples obtained from CC-0, CC-1, CC-2, CC-3 was denoted ACC-0, ACC-1, ACC-2, ACC-3.

2.2. Characterizations

The morphological characteristics and microstructure of each sample were characterized by scanning electron microscopy (SEM, ZEISS ULTRA PLUS) and X-ray diffraction spectrometry (XRD, PANalytical X Pertpro).The specific surface area and pore volumes of each sample were characterized by nitrogen adsorption-desorption (Micromeritics ASAP2020) at 77 K; the samples were degassed in a vacuum at 250°C for 2 h before analysis. Raman spectroscopy (Renishaw 2000) and X-ray photoelectron spectroscopy (XPS, Thermo ESCALAB 250XI) were used to describe the surface groups and graphitization of each sample.

2.3. Electrochemical measurements

The electrochemical properties were measured by a three-electrode system. With the ratio of 8:1:1 in weight, ACCs, conductive carbon black, polyvinylidene fluoride(PVDF) were mixed; then, appropriate amounts of dimethylacetamide solvent were added to the mixture above, coated on the nickel foam (10 × 10 × 0.5 mm) and dried in a vacuum drying box at 80°C for 12 h as working electrodes. The mass of each foamed nickel piece is about 0.2 g, and the quality of foamed nickel after coating is increased by about 25 mg. That means, the active ingredient of the carbon powder mixture of each electrode is about 25 mg. The thickness of the foamed nickel is almost constant before and after coating. The same size platinum sheet was used as a counter electrode, the saturated calomel electrode was used as a reference electrode, and 1 M NaCl was used as a liquid electrolyte. Cyclic voltammetry (CV) and electrochemical impedance spectroscopy (EIS) were assessed with an electrochemical work station (AlalisCHI660E) under the system described above.

The specific capacitance C can be calculated by the following equation [34]:

$$C = \int \frac{IdV}{2v\Delta Vm} \tag{1}$$

Here *C* represents the specific capacitance, *I* represent the current density, *V* is the potential, *v* is the potential scan rate, and m is the total mass of the electrode materials.

2.4. CDI experiments

The ACC-3, with polyvinylidene fluoride (PVDF) as the binder and conductive graphite powder as a conductive agent, was weighted in an 8:1:1 mixed ratio, dissolved in dimethylacetamide (DMAc, 99%) solvent, and then stirred for 12 h, followed by coating of the carbon slurry on the collector plate (graphite plate, 50 × 60 mm) at 80°C in the drying oven for12 h to form activated carbon coating electrodes. Finally, the electrodes were dried for 2 h in a vacuum dryer at 80°C to remove all organic solvent residues in the micropores of the electrode. The coated flow plate was fixed in a customized reactor and connected to a CDI process, as shown in Fig. 1. Based on our previous research experience, keep the plate-spacing at a distance of 2 mm, under a voltage of 1.4 V at 10 ml min^{-1} [35], the effluent conductivity profiles and pH curve with salt contents of 50, 100, 200, and 500 mg L^{-1} was tested, and the cycling performance was done to test the stability of the CDI cell after 10 salt adsorption and desorption cycles.

The salt adsorption capacity (SAC) of the electrodes can be calculated using the following equation:

$$SAC = \frac{C_1 - C_2}{m} \times V_{NaCl} \tag{2}$$

Here C_1 and C_2 are the initial and final concentrations of the NaCl aqueous solution. V_{NaCl} is the volume of the NaCl aqueous solution, and m is the whole mass of the electrode material coated onto the titanium plate.

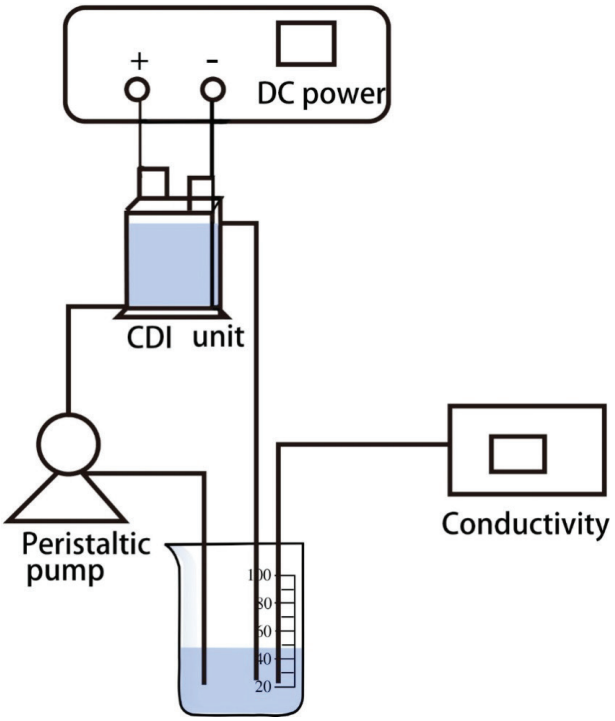

Fig. 1. Schematic diagram of the capacitance ionization unit used in the experiment.

3. Results and discussion

3.1. Morphological and structural characterizations

The microstructural and morphological features were characterized by scanning electron microscopy (SEM). Figs. 2 (a)–(f) show the typical structure of the ACC-1, ACC-2 and ACC-3. Because the raw material was directly crushed by corncob, and because the structure of the biomass is very different, the morphology of each sample was affected by the pore agent, which was also influenced by the original structure. We selected two typical structures of each sample and preliminarily judged the effect of the selection of the pore-making agent on the corncob sample. It can be seen from the SEM diagram that the samples ACC-1, ACC-2, ACC-3 had complex microstructures, and the etching effect of the pore-making agent on the biomass material was intuitively verified; the pore-making agent not only makes the original pores of the biomass more obvious but also produces a very rich microporous structure. A careful comparison showed that the ACC-1 and ACC-2 samples were more abundant, and the alkali vapour produced in the process of making holes helped form complex pores. With an appropriate voltage, this complex structure was conducive to the storage and adsorption of ions in a solution, forming a large capacity for the double electric layer capacitance, and this phenomenon can greatly improve the CDI process of salt adsorption.

The quantitative analysis of the pore structure was accomplished by the nitrogen adsorption-desorption experiment under 77 K. By comparing the adsorption isotherm of Fig. 3(a), we can see that the adsorption quantity increased rapidly with a lower surface pressure (p/p_0), and the adsorption was close to saturation in the p/p_0 = 0–0.1 interval, indicating that

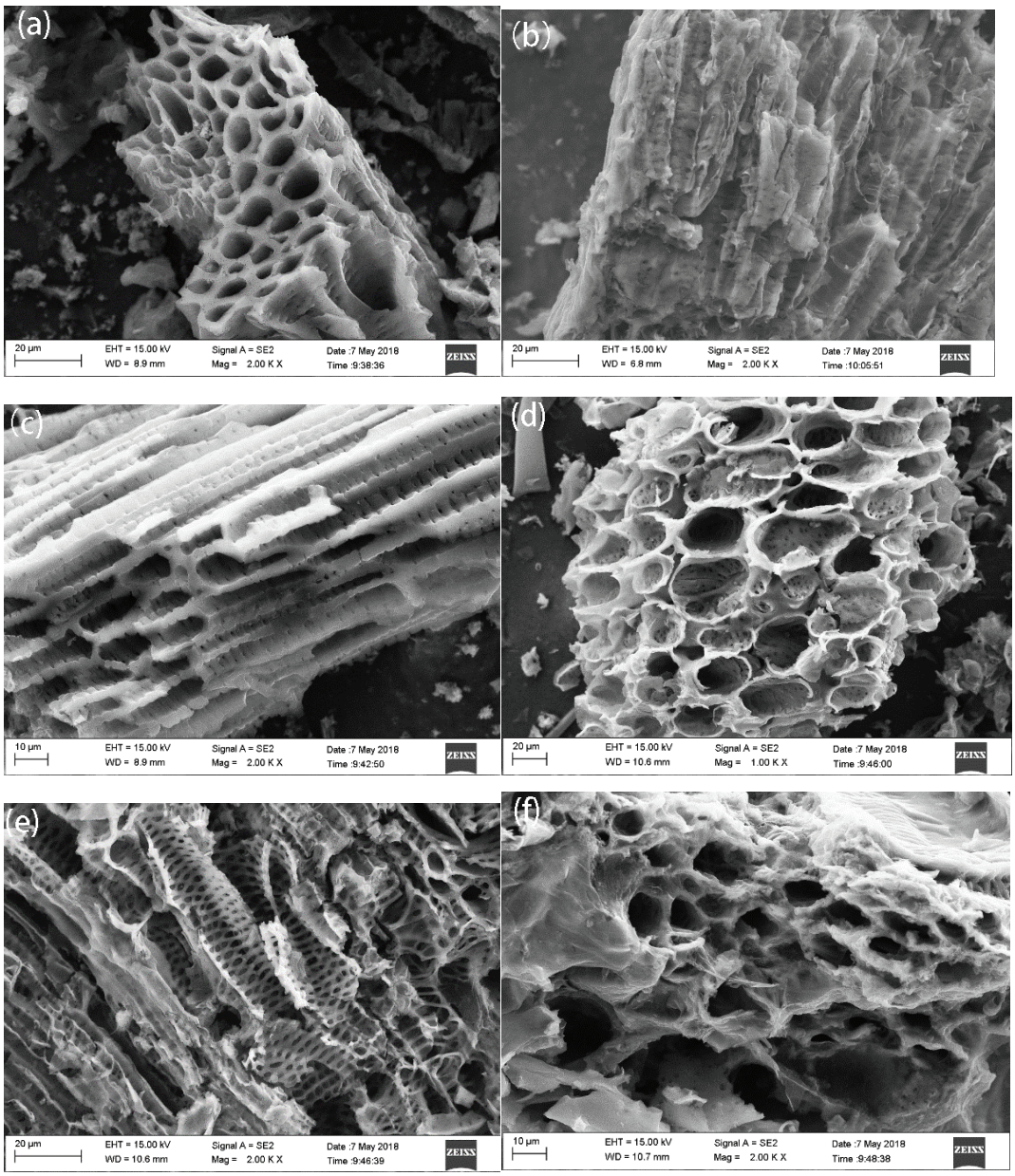

Fig. 2. Two typical SEM diagrams of samples ACC-1 (a,b), ACC-2 (c,d) and ACC-3 (e,f).

the material has abundant mesoporous and microporous structures [36]. The BET specific surface area of four kinds of material was calculated, and the BET specific surface area of the ACC-1 was 1,267.9 $m^2 g^{-1}$ and ACC-2 and ACC-3 were 1,093.4 and 384.5 $m^2 g^{-1}$.The ACC-0 with no pore-making agent showed a specific surface area of only 40.5 $m^2 g^{-1}$. Thus, the pore size obtained directly from SEM shows that the addition of the pore-making agent functions in the formation of a porous structure of corncob-based carbon material. Fig. 3(b) describes the pore size distributions of three groups using a hole-making agent according to the density functional theory (DFT); a richer micropore structure with the ACC-1 and ACC-2 is seen. The BET specific surface area and micropore distribution of the sample ACC-3 using $ZnCl_2$ as a hole-making agent are better than those without a pore-making agent, but there is still a large gap with the other two kinds of pore-making agents. The results verify that the microscopic morphology observed by SEM and the micropore distribution of samples ACC-1 and ACC-2 help form the double layer, and the selection of KOH and K_2FeO_4 is speculated to be advantageous for enhancing the adsorption capacity of CDI.

The degree of graphitization of ACC-1 and ACC-2 was characterized by XRD and Raman spectroscopy. According to the XRD spectra of Fig. 4(a), there was no obvious peak for sample ACC-1 that matched the amorphous carbon's XRD spectrum, and ACC-2 had obvious peaks near 2θ 26.5 and 44.4, which are assigned to typical (002) and (101) reflections of graphitic carbon (JCPDS no.41-1487).These results indicate that the addition of potassium ferrate leads to a certain graphitization transition of corncob carbon materials. The typical

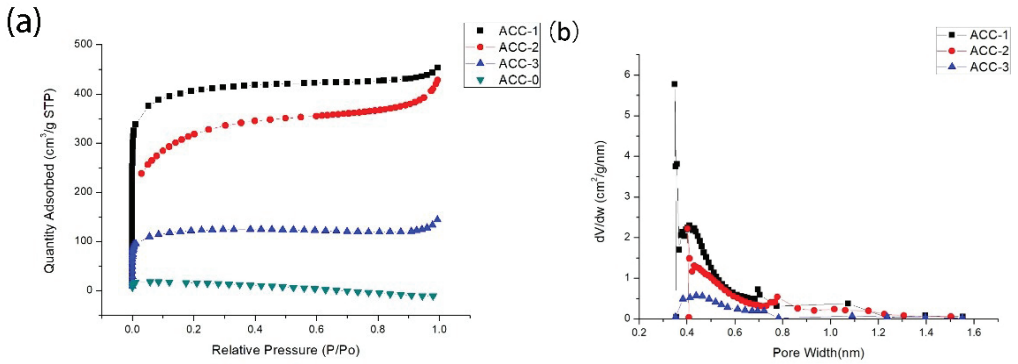

Fig. 3. N_2 Adsorption-desorption isotherm (a) and pore size distribution of each sample (b).

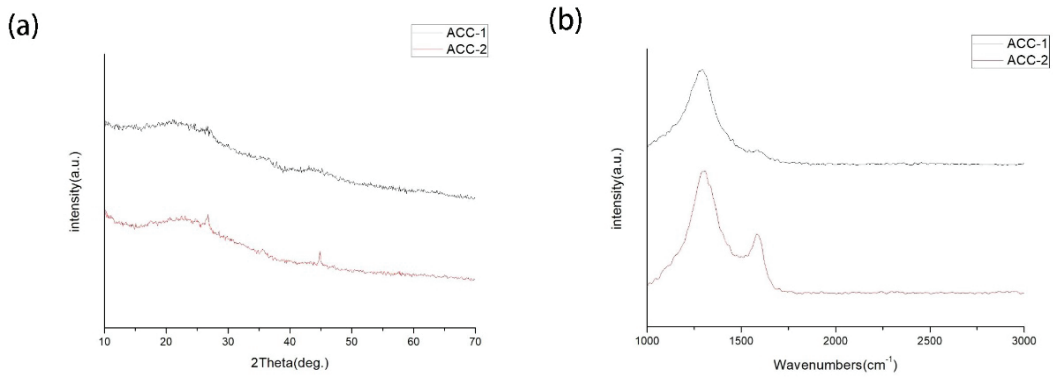

Fig. 4. XRD (a) and Raman (b) comparison diagram of theACC-1 and ACC-2 samples.

peaks, D-peaks and G-peaks, of the ACC-1 and ACC-2samples at wave lengths of 1,300 and 1,580 cm^{-1}, respectively, are obtained by the Raman spectra in Fig. 4(b). The intensity ratio of the *D* band to the *G* band (ID/IG) reacted to a defect in the degree of carbon material. *D*-peaks represent the defects in the *C*-atom lattice, and *G*-peaks represent the in-plane telescopic vibration of sp2 hybridization [37]. As seen in Fig. 4(b), both ACC-1 and ACC-2 had higher intensity *D*-peaks, suggesting that both the ACC-1 and ACC-2 samples can be categorized as amorphous carbon with more defects; however, ACC-2 demonstrates *G*-peak more obviously, which is an expression of the increased graphitization of the material. Therefore, we speculate that ACC-2 may have lower resistivity.

The surface functional groups of ACC-1 and ACC-2 were analysed by XPS to further describe the different chemical changes produced by the two pores formed during the carbonization of corncob. As shown in Fig. 5(a), there were only *C* and *O* elements on the surfaces of the ACC-1 and ACC-2 samples, and no other impurity elements were introduced. The C1s XPS spectrum of ACC-1 and ACC-2 was further fitted by the Gaussian–Lorentzian curve-fitting method (Figs. 5(b) and (c)).For the peak fittings, the background spectrum was removed by using the Shirley algorithm. From the control electron binding energy comparison table, the peak at 285.5 eV in Figs. 5(b) and (c), obtained by peaking, was a C–C sp2 hybridized peak, which is a highly oriented pyrolytic graphite (HOPG). The fit peak at 285.6 eV was a C–C sp3 hybridized peak, and the 287.8 eV fit peak was a carbon-oxygen double bond peak. A comparison between Figs. 5(b) and (c) indicated that the obvious decrease in the C–C sp3 peak area and the increase in the graphitized peak area further prove that the addition of potassium ferrate increased the degree of graphitization of the corncob-based carbon material. We can speculate that the oxygen element activated by the porous material with the corncob as the matrix exists mainly in the form of carbon-oxygen double bonds.

3.2. Electrochemical performance of the ACC electrodes

The electrochemical properties of the monolithic electrode were tested by the previously described three-electrode system. The cyclic voltammogram at different scan rates was used to verify the formation characteristics of the double layer in the corncob-based carbon material, and the capacitance was calculated from Eq. (1). The cyclic voltammetry curve obtained from the ACC-1sampleis shown in Fig. 6(a). With the scanning rates of 10, 20, 50, and 100 mv, the ACC-1 capacitances of the samples were 145.5, 128.2, 102.9, and 74.7 F g^{-1}, respectively. The cyclic voltammetry curve obtained by the ACC-2 sample is shown in Fig. 6(b), with capacitances of 141.5, 130.3, 101.1, and 72.3 F g^{-1} when the scanning rates were 10, 20, 50, and 100 mv s^{-1}, respectively. Figs. 6(a) and (b) show that the cyclic voltammetry curves of theACC-1 and ACC-2 samples were smooth, approximately rectangular and had some symmetry. With the 10 mv s^{-1} scanning rate, the cyclic voltammetry curve was closest to rectangular in shape. An increase in the scan rate caused the curve to deviate from the rectangle but retain the shape of a quasi-rectangle. This result is mainly due to the

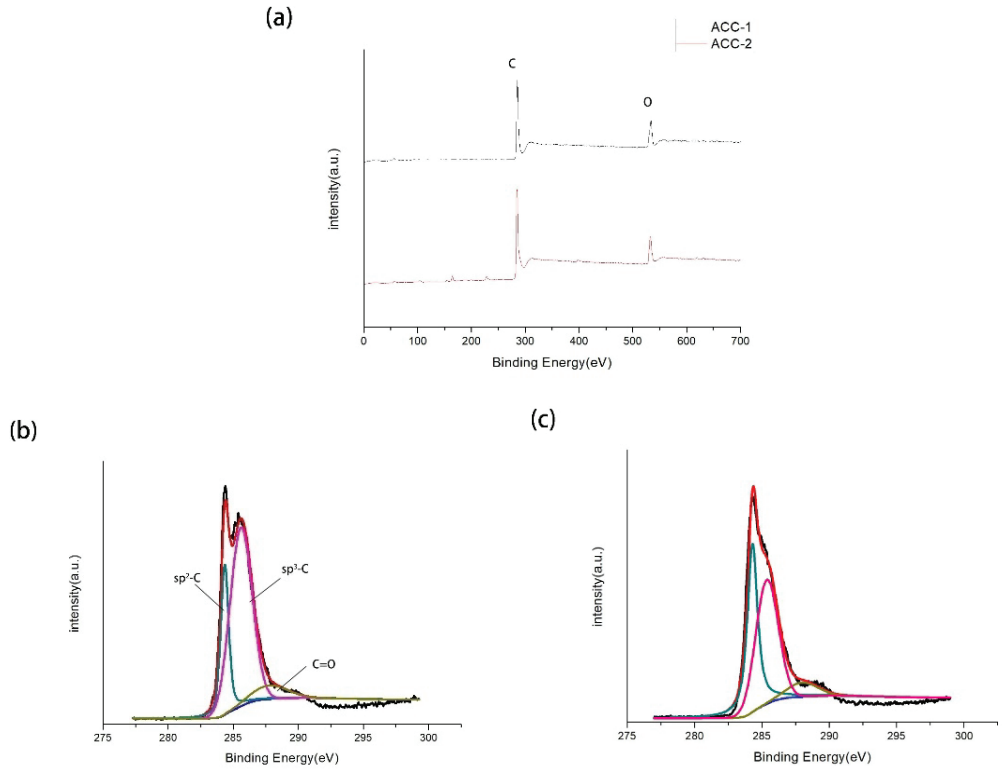

Fig. 5. XPS spectra of ACC-1 and ACC-2 (a) and C1s peak at high resolution (b,c).

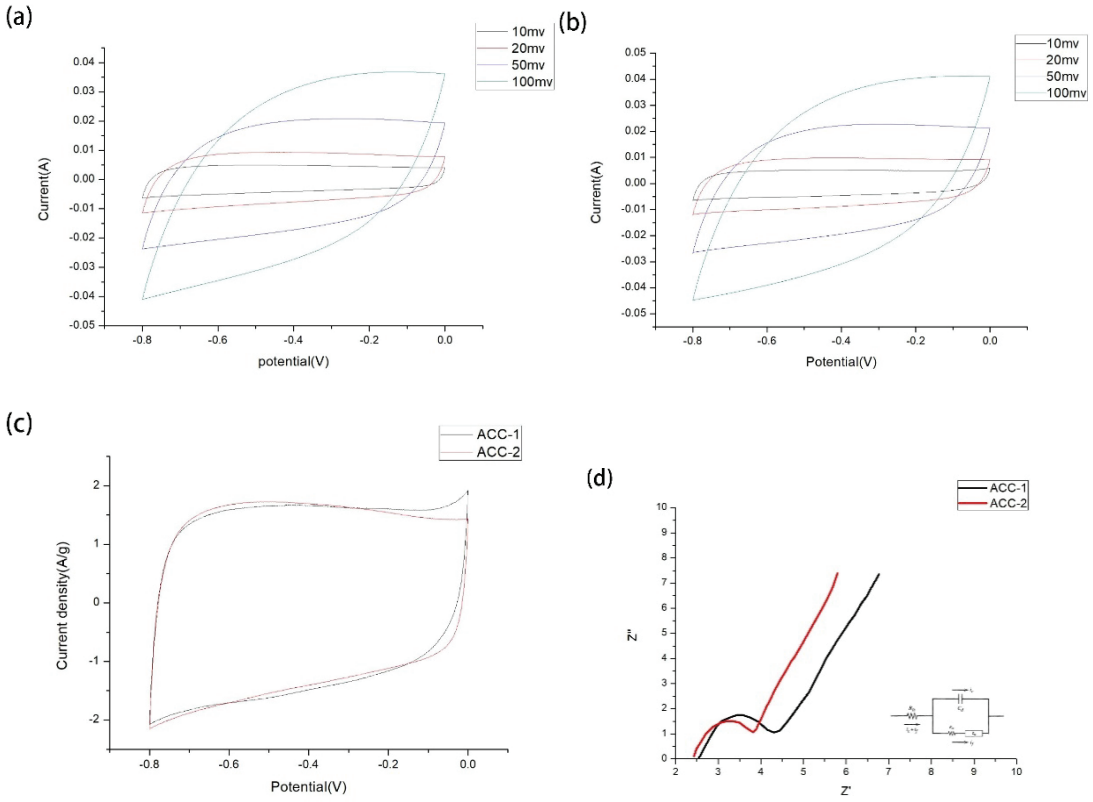

Fig. 6. CV curves with different scanning rates of ACC-1 (a) and the ACC-2 (b), and (c) the comparison of the energy density between ACC-1 and ACC-2 at a 10 mv scanning rate, (d) EIS (Nyquist plots) of ACC-1 and ACC-2 and their equivalent circuit diagrams.

existence of a decentralized capacitance effect, as the current needs a certain amount of time to achieve a steady state. The capacitance decreased with the increase in the scanning rate because the scanning rate was too fast and the pulse was too late to enter into the micro-pore of the activated carbon. The calculated capacitance values of ACC-1 and ACC-2 were quite similar, the selected scanning rate of the group of data was 10 mv, and the corresponding current value divided by quality compared with its energy density difference in Fig. 6(c) may provide insights into the energy density.

The internal resistance and the ion transport process of the biological carbon electrode were obtained from the AC impedance test and the Nyquist figure shown in Fig. 6(d), respectively; the equivalent circuit model of the Nyquist graph is shown in Fig. 6(d). In the low frequency region, the Nyquist plot of each electrode appeared as a straight line, indicating low ion diffusion resistance and low Warburg impedance. The time-period of the change in the high frequency region was so short that the material transfer did not occur, that is, the effect of the Warburg impedance ZW disappeared. The impedance of the entire system was affected by the internal resistance R_{Ω}, double-layer capacitance C_D and charge transfer resistance R_{ct}. R_{Ω} includes the inherent resistance of the electrode material, the ionic resistance of the electrolyte, and the contact resistance between the electrode and the current collector [38]. The R_{Ω} and R_{ct} of the ACC-1 were calculated to be approximately 2.46Ω and 0.96Ω, respectively, and the R_{Ω} and R_{ct} of the ACC-2 were approximately 2.51Ω and 1.12Ω, respectively. A comparison of the EIS spectra of the two samples showed that both charge transfer resistance and internal resistance of ACC-2 were lower than that of ACC-1, and the migration rate of ions in the ACC-2 system was more advantageous than that of ACC-1[39].

3.3. CDI performance

The adsorption quantity of the CDI unit with different pore-making agents in different concentrations of NaCl solution is shown in Fig. 7(a). Moreover, the detailed data of adsorption at each concentration are shown in Table 1, which shows that the adsorption capacities of the CDI electrodes prepared by two kinds of pore-making agents in a 500 mg L^{-1} solution were not significantly different. The pH of the influent water was 6.6 and the pH of the effluent was between 6.6 and 6.7. It can be considered that the pH did not change. It indicates that there was no electrochemical reaction occurred during the desalting process. The adsorption capacities for both agents were 16 mg g^{-1}, which is close to the adsorption quantity of various high-performance electrode materials in recent studies. Moreover, the experimental methods used in this experiment were of low cost. Fig. 7(a) also clearly reflects the increase in the adsorption of the electrodes as the concentration of the solution increases, which conforms to the Langmuir equation:

$$Q = \frac{Q_m KC}{1 + KC} \tag{3}$$

where C (mg L^{-1}) is the equilibrium concentration of NaCl, Q_m (mg g^{-1}) is the maximum electrosorption capacity, and K (mg L^{-1}) is the Langmuir constant.

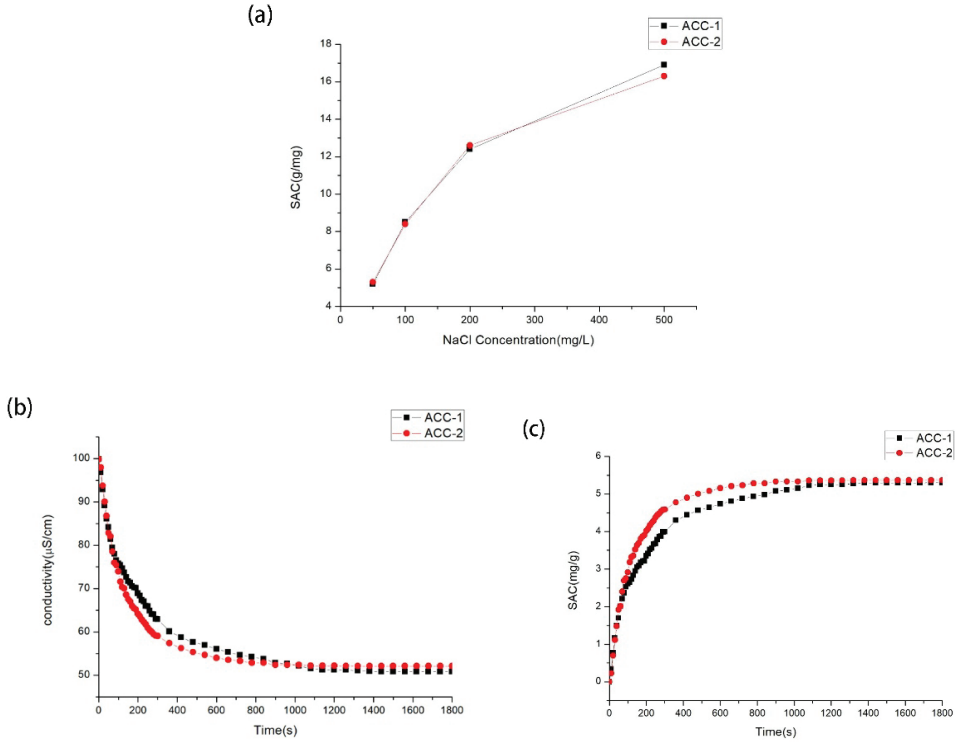

Fig. 7. (a) Comparison of the desalting performance of electrodes prepared with ACC-1 and ACC-2 at different NaCl concentrations, (b) time-dependent change of electrical conductivity of ACC-1 and ACC-2 at 50 mg L^{-1} NaCl concentrations, (c) change in the amount of desalted salt over time when the NaCl concentration was 50 mg L^{-1} for ACC-1 and ACC-2.

Table 1
Final desalting amounts of ACC-1 and ACC-2 at different concentrations and some key time-points during the desalination process

Concentration of NaCl (mg L^{-1})	Samples							
	ACC-1				ACC-2			
	50	100	200	500	50	100	200	500
SAC (mg g^{-1})	5.30	8.52	12.41	16.88	5.36	8.42	12.61	16.33
tSAC90% (min)	11	12	14	15	7	10	12	13
tSAC100% (min)	23	24	26	28	22	22	24	26

During the electrosorption process, we found that the K_2FeO_4 pore-forming electrode material was more easily adsorbed than the KOH-made electrode material. The time for the conductivity of the test solution of the ACC-1 electrode group did not change as fast as that of the ACC-2 group. Moreover, the time for the ACC-1 group to reach 90% of the total adsorption capacity was also faster than that of the ACC-2 group. Fig. 7(b) describes the decrease in conductivity over time at a solution concentration of 50 mg L^{-1}. The conductivity was recorded every 10 s for the first 5 min and every minute for 5–30 min. Fig. 7(b) visually shows that, in the ACC-1 electrode preparation apparatus, the conductivity decreased faster than that of the ACC-2 plate. Because the quality of the carbon material in the electrode plates of the ACC-1 and ACC-2 groups differed, the decrease in the conductivity did not fully reflect the size of the desalination rate. Therefore, the decrease in the conductivity at each point in Fig. 7(b) was calculated as the desalting capacity at each time in Fig. 7(c). The desalting capacity of the electrode prepared by ACC-1 in the first 20 min was found to be higher than that of the electrode prepared by ACC-2; the adsorption equilibrium was reached first, and the final adsorption amount was very close to that of the ACC-2 electrode. With other solution concentrations, the ACC-1 electrode reached the adsorption equilibrium sooner. The two key time points of the adsorption process are shown in Table 1, and NaCl at each concentration was able to achieve stability at 30 min in this experiment. Under the same conditions, using K_2FeO_4 pore-forming electrode materials can reduce the salinity in the solution more quickly. This phenomenon is related to the degree of graphitization of corn-based biochar increased effectively by K_2FeO_4 activation.

In cycling performance, we tested conductivity change diagrams of ten salt adsorption and desorption processes, and the conductivity of the nodes at each completion of the adsorption and desorption was marked in Fig. 8. It can be seen from Fig. 8. After each desorption process, the CDI modules composed of two materials can restore the ion concentration to the pre-adsorption level. It was demonstrated that the ions adsorbed in the pores of the plates during the desorption process can be almost completely desorbed back into the solution. In the process of multiple adsorption and desorption, there is a certain difference in the final value of the final decrease in the conductivity of the solution, but the difference is not large. The single cycle with the lowest amount of desorption was only less than 5% lower than the amount of desorption of the highest desorption, while the last cycle of desorption of material ACC-1 and ACC-2 was 96.4% and 96.9% of the first desorption cycle.

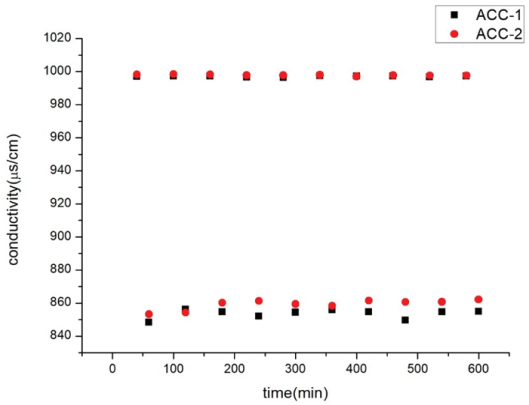

Fig. 8. Conductivity change diagram of ten adsorption and desorption.

4. Conclusion

Corncob waste allows the use of a simple treatment scheme to prepare carbon materials for CDI plates. The specific surface area of the prepared carbon powder reached 1,267.9 m^2 g^{-1}, and the capacitance in the three-electrode system reached 145.5F g^{-1}. The desalted adsorption capacity of brine in a 500 mg L^{-1} NaCl solution reached 16.9 mg L^{-1}. In this experiment, a low-cost method for producing a high-performance capacitive deionized electrode material was demonstrated while utilizing corncob waste as a resource. In this experiment, the influence of different pore-making methods on the microstructure of corncob activated carbon was described; the pore distribution of corncob carbon from K_2FeO_4 and KOH was better than that of other pore-making agents, and high adsorption capacity was achieved in the CDI desalination process. The use of KOH as a hole-making agent can result in a higher specific surface area of corncob activated carbon, and the medicament cost is lower than K_2FeO_4. Using K_2FeO_4 as an activated pore can effectively increase the graphitization degree of amorphous carbon, which may aid in decreasing the internal resistance of the CDI electrode. The change is helpful in increasing the time of adsorption equilibrium, and the adsorption quantity is equivalent to that of the plate material, which is activated by KOH. K_2FeO_4 is a promising new type of pore-making agent that can be used for preparing biological carbon electrodes. In the process of recycling 10 times, the adsorption performance did not decrease significantly, and the adsorption rate only decreased by about 3%, which can meet the requirements of repeated use.

Acknowledgements

This work was supported partly by the NSFC under Grant No. 51678188.

References

[1] Y. Oren, Capacitive deionization (CDI) for desalination and water treatment-past, present and future (a review), Desalination, 228 (2008) 10–29.
[2] M.A. Anderson, A.L. Cudero, J. Palma, Capacitive deionization as an electrochemical means of saving energy and dlivering clean water. Comparison to present desalination practices: will it compete?, Electrochim. Acta, 55 (2010) 3845–3856.
[3] M.E. Suss, S. Porada, X. Sun, P.M. Biesheuvel, Water desalination via capacitive deionization: what is it and what can we expect from it?, Energy Environ. Sci., 8 (2015) 2296–2319.
[4] M.A. Ahmed, S. Tewari, Capacitive deionization: processes, materials and state of the technology, J. Electroanal. Chem., 813 (2018) 173–192.
[5] G.X. Li, P.X. Hou, S.Y. Zhao, A flexible cotton-derived carbon sponge for high-performance capacitive deionization, Carbon, 101 (2016) 1–8.
[6] G. Wang, Q. Dong, T. Wu, Ultrasound-assisted preparation of electrospun carbon fiber/graphene electrodes for capacitive deionization: importance and unique role of electrical conductivity, Carbon, 103 (2016) 311–317.
[7] W. Kong, X. Duan, Y. Ge, Holey graphene hydrogel with in-plane pores for high-performance capacitive desalination, Nano. Res., 9(2016) 2458–2466.
[8] H. Li, Composite of hierarchical interpenetrating 3d hollow carbon skeleton from lotus pollen and hexagonal MnO_2 nanosheets for high-performance supercapacitors, J. Mater. Chem. A, 3 (2015) 9754–9762.
[9] X. Ye, Y. Zhu, Z. Tang, Z. Wan, C Jia, In-situ chemical reduction produced graphene paper for flexible supercapacitors with impressive capacitive performance, J. Power Sources, 360 (2017) 48–58.
[10] F. Duan, Y. Li, H. Cao, Capacitive deionization by ordered mesoporous carbon: electrosorption isotherm, kinetics, and the effect of modification, Desal. Wat. Treat, 52 (2014) 1388–1395.
[11] J. Zhang, J.H. Fang, J.L. Han, T.T. Yan, L.Y. Shi, D.S. Zhang, N, P, S co-doped hollow carbon polyhedra derived from MOF-based core–shell nanocomposites for capacitive deionization, J. Mater. Chem. A, 6 (2018) 15245–15252.
[12] J.L. Han, L.Y. Shi, T.T. Yan, J.P. Zhang, D.S. Zhang, Removal of ions from saline water using N, P co-doped 3D hierarchical carbon architectures via capacitive deionization, Environ. Sci. Nano, 5 (2018) 980–991.
[13] Z. Wang, T.T. Yan, G.R. Chen, L.Y. Shi, D.S. Zhang, High Salt Removal Capacity of Metal–Organic Gel Derived Porous Carbon for Capacitive Deionization, ACS Sustainable Chem. Eng., 5 (2017) 11637–11644.
[14] H.Y. Duan, T.T. Yan, G.R. Chen, J.P. Zhang, L.Y. Shi, D.S. Zhang, A facile strategy for the fast construction of porous graphene frameworks and their enhanced electrosorption performance, Chem. Commun., 53 (2017) 7465–7468.
[15] H. Wang, T.T. Yan, L.Y. Shi, G.R. Chen, J.P. Zhang, D.S. Zhang, Creating nitrogen-doped hollow Multiyolk@Shell carbon as high performance electrodes for flow-through deionization capacitors, ACS Sustainable Chem. Eng., 5 (2017) 3329–3338.
[16] S. Jeon, H. Park, J. Yeo, Desalination via a new membrane capacitive deionization process utilizing flow-electrodes, Energy Environ. Sci., 6 (2013) 1471–1475.
[17] J.Y. Lee, S.J. Seo, S.H. Yun, Preparation of ion exchanger layered electrodes for advanced membrane capacitive deionization (mcdi), Water Res., 45 (2011) 53–75.
[18] F.J. Álvarez-González, J.A. Martín-Ramos, J. Díaz, Energy-recovery optimization of an experimental cdi desalination system, IEEE Trans. Ind. Electron., 63 (2016) 1586–1597.
[19] A.M. Pernía, J.G. Norniella, J.A. Martín-Ramos, Up–down converter for energy recovery in a CDI desalination system, IEEE Trans. Ind. Electron., 27 (2012) 3257–3265.
[20] J. Kang, T. Kim, H. Shin, Direct energy recovery system for membrane capacitive deionization, Desalination, 398 (2016) 144–150.
[21] T. Wu, G. Wang, Q. Dong, Starch derived porous carbon nanosheets for high-performance photovoltaic capacitive deionization, Environ. Sci. Technol., 51 (2017) 9244–9251.
[22] D. Xu, Y. Tong, T. Yan, N, P-co-doped meso-/microporous carbon derived from biomass materials via a dual-activation strategy as high-performance electrodes for deionization capacitors, ACS Sustainable Chem. Eng., 5 (2017) 5810–5819.
[23] J.J. Lado, R.L. Zornitta, F.A. Calvi, M.I. Tejedor-Tejedor, Study of sugar cane bagasse fly ash as electrode material for capacitive deionization, J. Anal. Appl. Pyrolysis, 120 (2016) 389–398.
[24] J.J. Lado, R.L. Zornitta, F.A. Calvi, M. Martins, M.A. Anderson, F.G. Nogueira, L.A. Ruotolo, Enhanced capacitive deionization desalination provided by chemical activation of sugar cane bagasse fly ash electrodes, J. Anal. Appl. Pyrolysis, 126 (2017) 143–153.
[25] C.H. Hou, N.L. Liu, H.C. His, Highly porous activated carbons from resource-recovered Leucaena leucocephala wood as capacitive deionization electrodes, Chemosphere, 141 (2015) 71–79.
[26] Y. Liu, Z. Xiao, Y. Liu, Biowaste derived 3d honeycomb-like porous carbon with binary-heteroatom doping for high performance flexible solid-state supercapacitors, J. Mater. Chem. A, 6 (2017) 160–166.
[27] N. Rambabu, R. Azargohar, A.K. Dalai, Evaluation and comparison of enrichment efficiency of physical/chemical activations and functionalized activated carbons derived from fluid petroleum coke for environmental applications, Fuel Process Technol., 106 (2013) 501–510.
[28] E. Raymundo-Piñero, P. Cacciaguerra, T.D. Cazorla-Amorós, KOH and NaOH activation mechanisms of multiwalled carbon nanotubes with different structural organisation, Carbon, 43 (2005) 786–795.
[29] M.A Lillo-Ródenas, D. Lozano-Castelló, D. Cazorla-Amorós, Preparation of activated carbons from spanish anthracite: ii. activation by NaOH, Carbon, 39 (2001) 751–759.
[30] C. Saka, BET, TG–DTG, FT-IR, SEM, iodine number analysis and preparation of activated carbon from acorn shell by chemical activation with ZnCl2, J. Anal. Appl. Pyrolysis, 95 (2012) 21–24.
[31] M. Jagtoyen, F. Derbyshire, Activated carbons from yellow poplar and white oak by H_3PO_4 activation, Carbon, 36 (1998) 1085–1097.
[32] A.M. Dehkhoda, E. Gyenge, N. Ellis, A novel method to tailor the porous structure of KOH-activated biochar and its application in capacitive deionization and energy storage, Biomass Bioenergy, 87 (2016) 107–121.
[33] Y. Gong, D. Li, C. Luo, Highly porous graphitic biomass carbon as advanced electrode materials for supercapacitors, Green Chem., 19 (2017) 4132–4140.
[34] G. Wang, C. Pan, L. Wang, Q. Dong, Activated carbon nanofiber webs made by electrospinning for capacitive deionization, Electrochim. Acta., 69 (2012) 65–70.
[35] Y. Zhao, X.M. Hu, B.H. Jiang, L. Li, Optimization of the operational parameters for desalination with response surface methodology during a capacitive deionization process, Desalination, 336 (2014) 64–71.
[36] P.M. Biesheuvel, B.V. Limpt, A. Wal, Dynamic, adsorption/desorption process model for capacitive deionization, J. Phys. Chem. C, 113 (2009) 5636–5640.
[37] S.T. Jackson, R.G. Nuzzo, Determining hybridization differences for amorphous carbon from the XPS C 1s envelope, Appl. Surf. Sci., 90 (1995) 195–203.
[38] Y. Liu, X. Xu, M. Wang, T. Lu, Metal-organic framework-derived porous carbon polyhedra for highly efficient capacitive deionization, Chem. Commun., 51 (2015) 12020–12023.
[39] P. Biesheuvel, S. Porada, M. Levi, M. Bazant, Attractive forces in microporous carbon electrodes for capacitive deionization, J. Solid State Electrochem., 18 (2014) 1365–1376.